Proceedings of IMECE04
2004 ASME International Mechanical Engineering Congress and Exposition
November 13-20, 2004, Anaheim, California USA

IMECE2004-61955

ANALYTICAL MODEL DEVELOPMENT AND MODEL REDUCTION FOR ELECTROMECHANICAL BRAKE SYSTEM

Jaeho Kwak, Bin Yao*, and Anil Bajaj
School of Mechanical Engineering
Purdue University
West Lafayette, IN, 47907, USA
*Email: byao@purdue.edu

ABSTRACT

This paper presents a detailed analytical model development which can describe the dynamic behavior of the electromechanical brake-by-wire (BBW) system over the entire operating range. The complete model has 10 degree-of-freedom (DOF) and includes essential nonlinearities such as gear backlashes, Coulomb frictions, and disk gap clearance. Such a full model is reduced to 6 degree-of-freedom model in SIMULINK for simulation study of the effectiveness and the achievable performance of different hardware and controller designs, an invaluable tool in the early design stage of a product. Simulation results show that the model is able to reproduce various nonlinear characteristics including typical structural hysteresis as shown in real brake assembly.

The linearized version of the full nonlinear model is then obtained for its modal properties to understand the modes that are critical to the low frequency dynamics of the overall system. The results of the modal analyses are subsequently utilized to obtain two simplified models, one for non-contact mode and the other for the contact mode of operation. The concepts of two simplified models well capture the dynamic characteristics of the system over the frequencies of interest and are being used in the controller (e.g., clamping force control) and estimator (e.g., gap clearance estimation) designs that are under investigation.

1. INTRODUCTION

With regards to future vehicle concepts, the automotive industry is developing a fully electromechanical brake-by-wire (BBW) system as it allows reduced number of components, improvement in response times, and possibility of adding safety features such as anti-skidding through coordinated individual control of each brake. Especially, integration of ABS, Brake Assist, Traction, and Stability control becomes largely a matter of computer code, not of complex layers of addition hardware.

However, the BBW system demands more precise control than a conventional electrohydraulic brake system such as clamping force regulation to generate consistent braking force and disk gap management to avoid residual brake torque and pad wear. As a result, rigorous mathematical modeling plays a significant role in the development of the BBW system consisting of brushless DC motor, planetary gear train, roller screw drive, and floating brake caliper. Unfortunately, such a rigorous mathematical modeling has been lacking in the previous studies of BBW systems [1, 2, 5-7].

The aim of this paper is to develop in early design stage a reference model with relevant degrees of freedom. This model must describe the dynamic behavior of electromechanical brake components for the entire instrument range. Also, since there is a wide range of efficiency on the brake actuator due to changing environmental conditions (thermal, friction, and pad wear) and the nonlinearities (Coulomb friction, gear backlash, and brake gap clearance) of its components, the each wheel brake need to be operated in a clamping force feedback control and in a disk gap management [1, 3-5]. So, simplified models for future controller design and parameter estimator design are necessary.

The rest of this paper is organized as follows: Section 2 derives the complete nonlinear analytical model for an electromechanical brake system. From the developed full degrees of freedom model, natural frequencies and vibration modes are compared to capture the dominant frequency mode for the simplified model developed in Section 3. Then two simplified models for clamping mode and gapping mode defined by contacting condition (braking status) are developed in Section 4. In Section 5 the simulation results for the characteristics of complete nonlinear model and the validity of two simplified models are presented.

2. ANALYTICAL MODEL DEVELOPMENT

For the dynamic model development of electromechanical brake (Brake-by-wire) on a floating disk brake caliper, the structure [1, 2] consisting of brushless DC motor, planetary gear unit, roller screw drive and disk brake caliper is selected among various brake types and components [1-7]. This type of brake is made structurally stiff by fixing the nut carrier to the caliper housing through the use of the central bearing and by choosing roller screw drive instead of ball screw drive as shown in Fig. 1.

The aim of the model development is to provide a reference model which describes the behavior of the real brake for the entire instrument range. This reference model serves in initial design studies for feasibility and for aid in design. Also, it should possess sufficient accuracy to serve as a realistic nonlinear simulation test bed for design of a clamping force estimator and design of a controller.

2.1 Structure of the Benchmarked Brake [1]

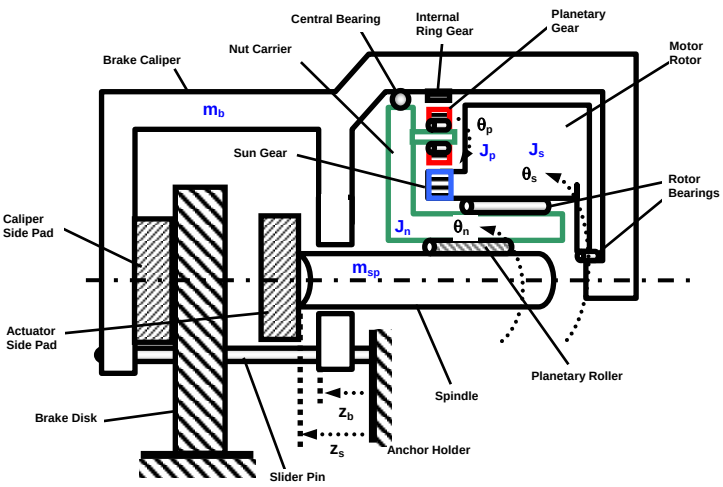

Figure 1. Layout for Electromechanical Disk Brake

The electromechanical brake is implemented based on the conventional floating caliper principle as shown in Fig. 1. With this principle, the anchor holder is firmly installed on the knuckle of the vehicle. The caliper housing with both pads floats through sliding pin with two degree-of-freedom in the interlocking of the clamping force. As an electromechanical converter, a brushless DC motor is used. The angular position of motor for the electrical commutation and for the regulation function is measured via an encoder. The cylinder shaped motor rotor is interlocked within the caliper housing and it is rigidly connected with the sun gear of the planetary gear unit. So, the moment of inertia of the rotor and the sun gear will be lumped together in the following modeling. The planet gear of the planetary gear unit is in mesh with the sun gear and with the internal ring gear that is bolted in the brake caliper housing and propels the nut carrier. To convert the rotation of the planetary gear into a linear movement for the necessary clamping force of the brake caliper assembly, a roller screw drive is used. In the operation of the brake, the actuator-side brake pad is shifted by the spindle of the roller screw drive in the moving direction of the disk brake. As soon as the actuator-side pad comes in contact with the brake disk rotor, the entire brake housing floats until the required clamping force is generated. Here, the central bearing of the nut carrier supports a radial force as well as a axial force to react against the clamping force. So the large axial clamping force is immediately absorbed by the nut-screw mechanism without transferring down to the motor and gear unit. A combination of ball bearings and roller bearings makes possible the relative rotation between the motor rotor and the screw nut, as shown in Fig. 1 and Fig. 2. For the further radial support of the drive unit, a roller bearing is intended between the encoder rotor and the encoder stator.

2.2 Dynamic Model

2.2.1 Planetary Gear Train (PGT)

To meet the required power and high torque needs within space constraints, planetary gear trains have been widely used in aerospace and automotive applications. They help amplify the force/torque that can be produced by an electronic motor. In addition to being compact in size and physical construction, high efficiency and low sensitivity to shock loading also make the planetary gear train (PGT) attractive for electromechanical brakes. However, the dynamic behavior of a PGT is very complex due to the nonlinear effects such as backlash, the variation of gear mesh stiffness and damping, and various frictions as well as the complex motion of the planetary gear which generates revolution and rotation movement at the same time. For example, the modeling of dynamic tooth forces still remains as important issue that has not been resolved even for single-mesh PGT. Dynamic analysis including the prediction of natural modes and gear mesh forces has been one of the major research area for planetary gear trains [8-13]. For simplified PGT dynamic analysis in most researches, however, an equivalent conventional gear train concept or a carrier fixed PGT is used to remove the relative motion caused by nut carrier rotation [9, 10], or a purely torsional model is used ignoring the bearing stiffness between planetary gear and nut carrier pin [12, 13]. This section details the dynamic model development a PGT including the movement of relative motion and the bearing stiffness aimed at exploring the dynamic behavior of power transmissions.

Formulation

In the electromechanical brake, the single stage PGT is considered. It consists of a sun gear connected with motor rotor, an internal ring gear fixed with caliper housing, and 3 identical planetary gears coupling the sun gear with the internal ring gear, as shown in Fig. 2. The planetary gears are mounted on the rigid nut carrier through bearings and pins. In the present usage of the PGT, the sun gear is the input and the nut carrier thrusting the spindle is the output of the PGT unit. In the technical model development, the planetary gear dynamics can be simplified for the purpose of this paper. However, the contacting dynamics (the stiffness of bearing or gear mesh) lying in the power train cannot be neglected in relation to the stiffness of the other brake components during the development stage of the electromechanical brake system. For this reason, in the following, the PGT unit will be modeled as an eight degree-of-freedom (DOF) system without translational spindle

movement as shown in Fig. 2. The following assumptions are also made in developing the dynamic model of the PGT:

1) The gear wheels and the nut carrier are assumed to be rigid bodies.
2) The gear flexibilities are modeled as averaged linear gear mesh springs and dampers acting on the plane of the motion.
3) XY-axis is a fixed coordinate, i.e., the lateral movement of the caliper will be ignored.
4) x_iy_i-axis is the moving coordinate system attached to the center of the planetary gear i (i=1~3) and moving with it.

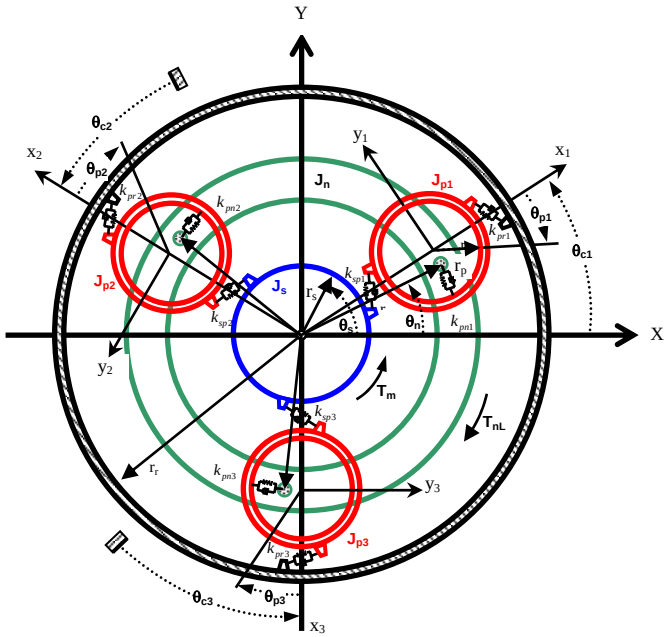

Figure 2. PGT Model for Rotational Dynamics

Basic Equation of Motion for PGT

The angular displacements of central members θ_s, θ_{ci} (i=1~3), and θ_n are defined as absolute displacements about a fixed coordinate frame while the angular displacements of planets θ_{pi} are defined relative to the carrier with positive direction along the negative z_i-axis of the moving coordinate systems $x_iy_iz_i$ which are related to the absolute angular displacement of planetary gear θ_{pci} as

$$\theta_{pci} = \theta_{ci} - \theta_{pi} \quad \text{or} \quad \theta_{pi} = \theta_{ci} - \theta_{pci} \tag{1}$$

To derive the basic equations of motion for PGT only, the Lagrange's method neglecting damping is employed. Thus

$$L = \frac{1}{2}[J_s\dot{\theta}_s^2 + \sum_{i=1}^{3} J_{pi}(\dot{\theta}_{ci} - \dot{\theta}_{pi})^2 + \sum_{i=1}^{3} m_{pi}(r_n\dot{\theta}_{ci})^2 + J_n\dot{\theta}_n^2]$$
$$-\frac{1}{2}[\sum_{i=1}^{3} k_{spi}(r_s\theta_s - r_s\theta_{ci} - r_{pi}\theta_{pi})^2 + \sum_{i=1}^{3} k_{pri}(r_{pi}\theta_{pi} - (r_n + r_{pi})\theta_{ci})^2 + \sum_{i=1}^{3} k_{pni}r_n^2(\theta_{ci} - \theta_n)^2] \tag{2}$$

The Lagrange's equations of motion for PGT only are given as

$$\frac{d}{dt}\left(\frac{\partial L}{\partial \dot{\theta}_j}\right) - \frac{\partial L}{\partial \theta_j} = Q_j \tag{3}$$

where $j = s, p1, c1, p2, c2, p3, c3, n$, and only the generalized forces $Q_s = T_m$ (motor torque) and $Q_n = -T_{nL}$ (nut load to next step) exist. Eq. (3) in conjunction with Eq. (2) yields eight ordinary differential equations given below: (i=1~3)

$$J_s\ddot{\theta}_s + r_s^2\sum_{i=1}^{3} k_{spi}\theta_s - r_s\sum_{i=1}^{3} r_{pi}k_{spi}\theta_{pi} - r_s^2\sum_{i=1}^{3} k_{spi}\theta_{ci} = T_m \tag{4}$$

$$J_{pi}(\ddot{\theta}_{pi} - \ddot{\theta}_{ci}) - k_{spi}r_sr_{pi}\theta_s + (k_{spi} + k_{pri})r_{pi}^2\theta_{pi} + (k_{spi}r_sr_{pi} - k_{pri}r_{pi}(r_n + r_{pi}))\theta_{ci} = 0 \tag{5}$$

$$(J_{pi} + m_{pi}r_n^2)\ddot{\theta}_{ci} - J_{pi}\ddot{\theta}_{pi} - k_{spi}r_s^2\theta_s + (k_{spi}r_sr_{pi} - k_{pri}r_{pi}(r_n + r_{pi}))\theta_{pi} + (k_{spi}r_s^2 + k_{pni}r_n^2 + k_{pri}(r_n + r_{pi})^2)\theta_{ci} - k_{pni}r_n^2\theta_n = 0 \tag{6}$$

$$J_n\ddot{\theta}_n - r_n^2\sum_{i=1}^{3} k_{pni}\theta_{ci} + r_n^2\sum_{i=1}^{3} k_{pni}\theta_n = -T_{nL} \tag{7}$$

In this section, the damping term and nonlinear terms such as Coulomb friction and backlash are not presented for the simple expression. Complete nonlinear models including the terms are derived in Appendix [A].

2.2.2 Conversion by Roller Screw Drive

To convert a rotatational motion into a linear movement, a set of mechanical components are available with different working principles. For electromechanical brakes, a planetary roller screw drive with reduction is particularly suitable due to its high load-carrying capacity, its small building area, its small pitch and high rotating speed. The main components are the nut carrier, the spindle to lead thread rolling, and rollers. With a rotatational motion of the nut, the rollers move in radial and axial direction. Each roller is led back after a circulation. The planetary roller screw drive can be simplified as a two-mass model ignoring the inertia of the roller between nut carrier and spindle as shown in Fig. 1 and Fig. 2. On the assumption of a rigid planet nut carrier for the brake modeling, the rotation angle of the screw nut carrier equals to the rotation angle of the planet nut carrier, and the planet nut carrier load torque is related to the equivalent driving axial force actuating the spindle by

$$T_{nL} = \left(\frac{p}{2\pi}\right)F_{ns} \tag{8}$$

where p is the pitch of the roller screw, and F_{ns} is the equivalent axial force to actuate the spindle in the actuation direction of the disk brake. With the contacting stiffness K_{ns} and the contacting damping C_{ns}, the axial force F_{ns} can be calculated from the rotation angle of the nut carrier θ_n, the spindle axial displacement z_s, the brake caliper displacement z_b and their derivatives as described in Eq. (9).

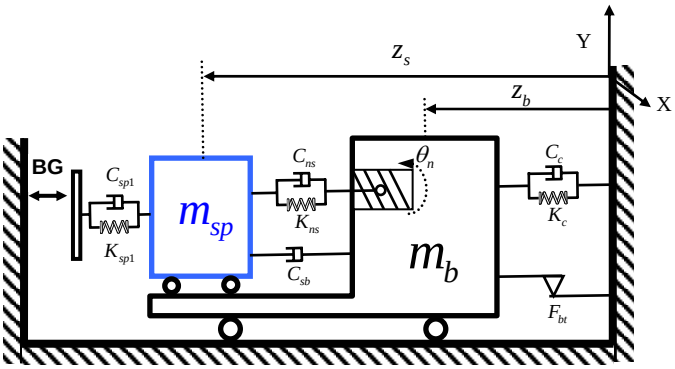

Figure 3. Friction Assembly for Translational Movement

2.2.3 Floating Disk Brake Assembly

The floating saddle friction assembly is modeled as a two-degree-of-freedom lumped mass-spring-damper system as shown in Fig. 3, in which different model equations and model parameters should be used according to the gaps between the two pads and the rotor. In this paper, the brake caliper dynamics are considered as a 2-phase model because the gap between the caliper side pad and the disk rotor is relatively very small when compared with the gap between the actuator side pad and the brake disk rotor (seeFig.1 and Fig. 3). Also, the following conditions are assumed in the theoretical model development:

1) Brake disk rotor is assumed to be a fixed (rigid) body because its stiffness is very high in relation to the stiffness of the other brake components.
2) The axial stiffness of central bearing is ignored in relation to the stiffness of the other brake components during clamping mode.
3) The brake caliper is assumed as a lumped mass m_b attached to the fixed disk rotor through a spring with a lumped stiffness of K_c and a lumped damping C_c.

Equation of Motion for Spindle Dynamics ($z_s \geq BG$)

From Fig. 3, the spindle dynamics is presented as

$$m_{sp}\ddot{z}_s + C_{sb}(\dot{z}_s - \dot{z}_b) + F_{sp1} - F_{ns} = 0 \qquad (9)$$

where

$$F_{sp1} = K_{sp1}(z_s - BG) + C_{sp1}(\dot{z}_s)$$

$$F_{ns} = K_{ns}(\frac{p}{2\pi}\theta_n + z_b - z_s) + C_{ns}(\frac{p}{2\pi}\dot{\theta}_n + \dot{z}_b - \dot{z}_s)$$

Equation of Motion for Brake Caliper ($z_s \geq BG$)

The brake caliper mass is actuated by the transmission forces described in Fig. 3. Then,

$$m_b\ddot{z}_b + C_{sb}(\dot{z}_b - \dot{z}_s) + K_c z_b + C_c\dot{z}_b - F_{bt} + F_{ns} = 0 \qquad (10)$$

The caliper friction force F_{bt} is mainly due to the lateral force between the caliper and sliding pin caused by the brake friction force between the rotor and the brake pad. As such, it consists of a static component and a component that is proportional to the total clamping force, and is assumed to be modeled by

$$F_{bt} = -\text{sgn}(\dot{z}_b)\left(F_{bt0} + \mu_b \cdot \mu_c \cdot \left|F_{sp1}\right|\right) \qquad (11)$$

where F_{bt0} is the static friction between the caliper and slider pin, μ_b is the friction coefficient between the pad and the disk rotor, and μ_c is the friction coefficient between the caliper and the sliding pin.

The complete analytical models including damping, Coulomb friction, backlash, and brake gap clearance are derived in Appendix [A] and implemented in SIMULINK as shown in Fig. 11. Their complete nomenclature and values are listed in Appendix [B].

3. NATURAL FREQUENCY AND VIBRATION MODE

In this section, several modal analyses are developed based on natural frequency and vibration mode shapes without nonlinear effects. These analyses have a useful geometric interpretation in early design stage of electromechanical brake system for tuning resonances away from operating speeds and optimizing the structural design. Also, through these analyses, a reduced order planetary gear train (PGT) model will be derived by removing modes of higher frequencies so as to avoid using a model with unnecessary a large number of degrees of freedom.

We begin with the determination of the natural frequencies and mode shapes for only the 8-DOF PGT model without translational brake assembly. The 8-DOF PGT model is subsequently reduced into the 4-DOF model of PGT through natural frequency and mode shape analysis. In section 4, this reduced PGT model will be then integrated with the spindle dynamics and the caliper dynamics to form the 6-DOF brake model to investigate the natural frequencies and mode shapes of the entire brake system during the two distinct operating conditions respectively: gapping mode before the pad makes contact with the rotor and clamping mode thereafter.

3.1 Full PGT Model

The natural frequencies and mode shapes of the 8–DOF PGT model when the planet nut carrier is not constrained (i.e. $T_{nL} = 0$), are obtained by solving the free vibration eigenvalue problem from the derived equations, Eq. (4) to Eq. (7) ignoring damping terms. All planetary gears are assumed identical and equally spaced with equal sun-planet mesh stiffness, ring-planet mesh stiffness, and planetary gear-nut bearing stiffness. The obtained natural frequencies and mode shapes given in Fig. 4 reveal several characteristics that can be classified into three groups: a rigid body mode, planet modes, and an overall mode [10] as follows:

Rigid Body Mode: So long as the input and output members are not constrained, the stiffness matrix is semi-definite resulting in a “rigid body” mode at zero frequency, as is shown in Fig. 3(a). In this mode, all gears rotate as rigid bodies without any gear or bearing mesh deflections. Hence, the

following kinematic relationships are obtained when only rigid body mode is considered:

$$\theta_{ci} = \theta_n \quad \text{where (i=1~3)} \tag{12}$$

$$\theta_{pi} = \frac{(r_s + 2r_{pi})\theta_{ci}}{r_{pi}} \tag{13}$$

$$\theta_s = \frac{2(r_s + r_{pi})}{r_s}\theta_{ci} \tag{14}$$

From the above equations, the overall gear ratio of the PGT is calculated as

$$N_{tot} = \frac{\theta_s}{\theta_n} = \frac{2(r_s + r_{pi})}{r_s} = \frac{r_s + r_r}{r_s} \tag{15}$$

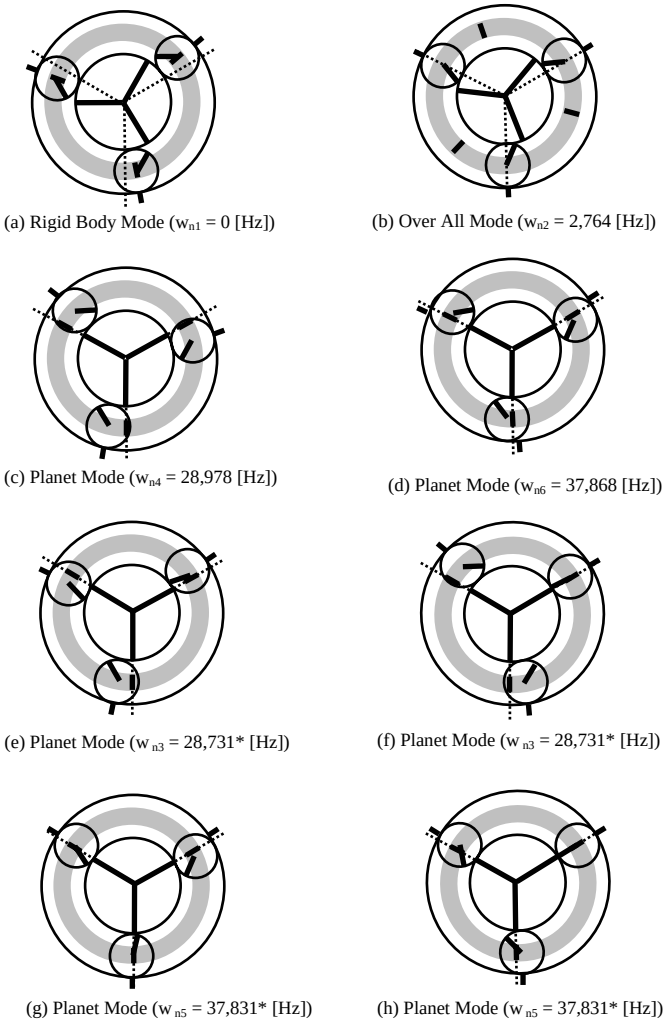

(a) Rigid Body Mode (w_{n1} = 0 [Hz]) (b) Over All Mode (w_{n2} = 2,764 [Hz])

(c) Planet Mode (w_{n4} = 28,978 [Hz]) (d) Planet Mode (w_{n6} = 37,868 [Hz])

(e) Planet Mode (w_{n3} = 28,731* [Hz]) (f) Planet Mode (w_{n3} = 28,731* [Hz])

(g) Planet Mode (w_{n5} = 37,831* [Hz]) (h) Planet Mode (w_{n5} = 37,831* [Hz])

Figure 4. Natural Mode Shapes for Full PGT Model

Planet Modes: These are the asymmetric modes at the double mode frequencies w_{n3}* and w_{n5}*, as shown in Fig. 4 (e-h), as well as the axi-symmetric modes at the modal frequencies w_{n4} and w_{n6} as shown in Fig. 4 (c, d) characterized by motions of planets relative to each other. At these modes, only the planetary gears move with respect to each other such that the input sun gear and the output nut carrier do not move. Also, at the multiple double mode frequencies (asymmetric), the summation of modal amplitude is zero.

Over All Mode: Besides the rigid body mode and the planet modes, there is a third mode at the frequency, w_{n2} as shown in Fig. 4(b). At this mode, all planets move exactly the same way forming an axi-symmetric mode shape to generate the non-zero displacements of the input and output members. This type of mode is the so-called "overall mode". It is characterized by existence of vibrations of all PGT members in contribution to the overall motion.

3.2 Reduced PGT Model

In general, the PGT with equally spaced three identical planetary gears (i.e., $J_{p1} = J_{p2} = J_{p3}$, $m_{p1} = m_{p2} = m_{p3}$), has both the symmetric modes that contribute to the overall input-output motion and that generate relative internal motion of planets only. Thus, if only the input-output motion of the PGT unit is of concern, as is the case in subsequent study of the overall brake dynamics, the axi-asymmetric double modes can be ignored for simplicity. As a result, all planets have the same motion, i.e., $\theta_{p1} = \theta_{p2} = \theta_{p3} = \theta_p$, and $\theta_{c1} = \theta_{c2} = \theta_{c3} = \theta_c$, and can be simplified as a lumped planet having inertia and stiffness property model by relations:

$$J_p = \sum_{i=1}^{3} J_{pi} \quad \text{and} \quad m_p = \sum_{i=1}^{3} m_{pi} \tag{16}$$

$$k_{sp} = \sum_{i=1}^{3} k_{spi}, \quad k_{pr} = \sum_{i=1}^{3} k_{pri} \quad \text{and} \quad k_{pn} = \sum_{i=1}^{3} k_{pni} \tag{17}$$

Subsequently, the number of DOF of the overall PGT unit reduces to four: $\theta_s, \theta_p, \theta_c,$ and, θ_n and the governing linear dynamic equations are simplified. By solving the free vibration eigenvalue problem for the reduced PGT, natural frequencies and mode shapes of the reduced 4–DOF PGT unit are obtained as shown in Fig. 5.

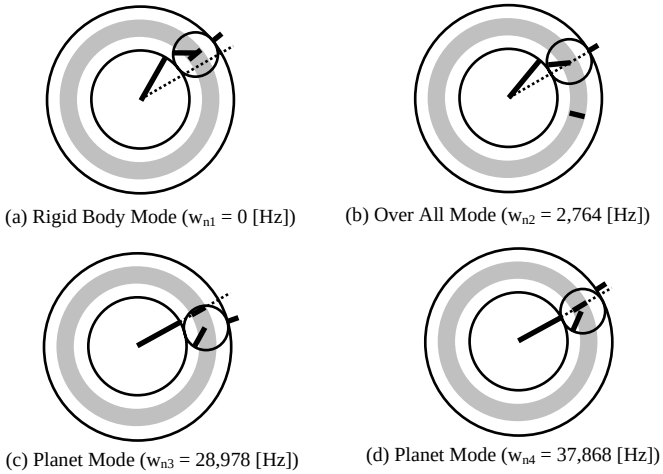

(a) Rigid Body Mode (w_{n1} = 0 [Hz]) (b) Over All Mode (w_{n2} = 2,764 [Hz])

(c) Planet Mode (w_{n3} = 28,978 [Hz]) (d) Planet Mode (w_{n4} = 37,868 [Hz])

Figure 5. Natural Mode Shapes for Reduced PGT Model

The obtained natural frequencies and mode shapes for the reduced PGT model reveal the same characteristics with the full PGT model that can also be classified into three groups: a rigid body mode, planet modes, and an overall mode. As expected, the natural frequencies and mode shapes of the two planet modes of the reduced PGT model are exactly the same as the two axi-symmetric modes of the full PGT model. This reduced 4-DOF PGT model is especially useful to simplify the simulation program.

4. SIMPLIFIED MODEL

In section 3 and Appendix [A], several analytical models including nonlinearities were developed which describe the dynamic behavior of an electromechanical disk brake with high accuracy for simulation based analysis and design purposes. For the analytical design of estimators and feedback controllers, it is however not meaningful to use the model in its full complexity. Rather, the model structure and the number of parameters to be dealt with can be further reduced based on the dominant factors analyzed in previous sections.

According to status of braking system, simplified models for gapping mode and for clamping mode are respectively developed in this section. The derived simplified clamping mode and gapping mode models are then used to construct estimation algorithms for clamping force and spindle position in respect based on the measurement of motor position via encoder and the motor current. Note that in the ideal case, the contacting position between the disk rotor and the pad is known. In addition, an analytical formula that relates the dominant mode of overall modes is developed. This formula provides estimate to the lowest natural frequency, from which the major parameters influencing the lowest natural frequency in clamping mode is clearly identified. This information is very useful in the early design stage of the prototype brake system.

4.1 Clamping Model

During the clamping mode the spindle (actuator side pad) makes contact with the brake rotor, disk as shown in Fig. 1 and Fig. 3. In addition to the reduced PGT model shown in Fig. 5, the translational spindle dynamics, Eq. (9), and caliper dynamics Eq. (10), can be incorporated into a 6-DOF clamping model. For the clamping model, the natural frequencies are obtained by solving the free vibration eigenvalue problem as shown in Table 1.

Table 1. Natural Frequencies for Clamping Mode Model

	w_{n1}	w_{n2}	w_{n3}	w_{n4}	w_{n5}	w_{n6}
Hz	**5**	1080	2764	12894	28978	37868

In this paper, we only have to consider the lowest flexible mode around 5 [Hz] in the estimator and controller design as the frequencies of all other modes are above 1 [kHz]. The lowest mode is concerned with the translational movement of friction assembly. Therefore, the rotational movement of planetary gear train (PGT) can be lumped together as a rigid body motion. Consequently, when ignoring load friction losses, total equivalent mass m_{beq} reflected to translational brake movement can be obtained as:

$$m_{beq} = m_b + m_{sp} + \left(J_n + m_p r_n^2\right)\left(\frac{2\pi}{p}\right)^2 + J_p\left(\frac{2\pi}{p}\right)^2\left(\frac{2r_p}{r_s}\right)^2 + J_s\left(\frac{2\pi}{p}\right)^2\left(\frac{2r_n}{r_s}\right)^2 \tag{18}$$

The corresponding values of Eq. (18) based on the nominal parameter values of brake assembly are presented in Table 2. As presented in Table 2, the equivalent mass of sun gear which is amplified by the square of gear ratio and pitch ratio is most dominant whereas spindle mass and caliper mass are negligible where compare to total equivalent mass. From Fig. 3, therefore, the translational brake assembly can be assumed as a series combination of springs without mass ignoring friction losses, as is shown in Fig. 6. Also, from Eq. (9), the clamping force F_{sp1} when ignoring friction losses, is defined as same as the nut-spindle transfer force F_{ns}:

$$F_{ns} \cong F_{sp1} \tag{19}$$

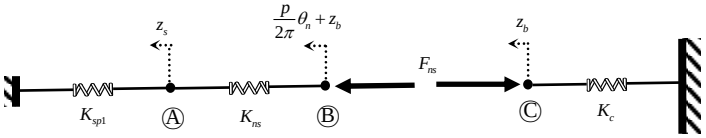

Figure 6 Translational Movement of Brake Assembly containing Massless Junction

Table 2. Equivalent Mass Reflected to Translational Brake Assembly Movement

Mass reflected to brake movement		Value [kg]
m_b	(brake caliper)	6.41
m_{sp}	(spindle with pad)	0.54
$J_n(2\pi/p)^2$	(nut carrier)	5612.95
$m_p r_n^2(2\pi/p)^2$	(translational planetary gear)	420.43
$J_p(2\pi/p)^2(2r_p/r_s)^2$	(rotational planetary gear)	20.45
$J_s(2\pi/p)^2(2r_n/r_s)^2$	(sun gear)	31360.70
m_{beq}		**37421.48**

From the equilibrium forces at massless junctions Ⓐ, Ⓑ, and Ⓒ, and rigid PGT assumption, the clamping force can be defined by an equivalent spring constant terms the motor angle:

$$F_{ns} = K_{eq}\left(\frac{p}{2\pi}\right)\left(\frac{r_s}{2r_n}\right)\theta_s \tag{20}$$

where

$$K_{eq} = \frac{K_{sp1}K_{ns}K_c}{K_{sp1}K_{ns} + K_{ns}K_c + K_{sp1}K_c}$$

So, the lowest mode can be obtained analytically by Eq. (18) and Eq. (20) to have the natural frequency.

$$w_{n1} = \sqrt{\frac{K_{eq}}{m_{beq}}} = 4.95\,[Hz] \tag{21}$$

Since this frequency is close to the lowest modal frequency of Table 1, the assumption of massless series spring as shown in Fig. 6 is reasonable. Therefore, a simplified clamping model reflected to the sun gear (motor angle) can be obtained by the rigid body assumption of PGT in rotational movement and the series spring assumption of friction assembly in translational movement. Thus,

$$J_{ceq}\ddot{\theta}_s = T_m - C_{ceq}\dot{\theta}_s - \mathrm{sgn}(\dot{\theta}_s)\bullet M_{ceq0} - K_{eq}\left(\frac{p}{2\pi}\right)^2\left(\frac{r_s}{2r_n}\right)^2\theta_s \tag{22}$$

4.2 Gapping Model

The situation when the spindle (actuator side pad) makes no contact with the brake disk rotor, as shown in Fig. 1 and Fig. 3, is referred to as the gapping mode in this paper. This equation governing for system behavior during the gapping mode can be obtained by setting $K_{sp1} = 0,\ C_{sp1} = 0, \text{and } F_{sp1} = 0$ in Eq. (9). The natural frequencies for gapping mode operation are obtained by solving free vibration eigenvalue problem for the no constrained system. These frequencies are given as shown in Table 3.

Table 3. Natural Frequencies for Gapping Mode Model

	w_{n1}	w_{n2}	w_{n3}	w_{n4}	w_{n5}	w_{n6}
Hz	**0**	**395**	2764	**12375**	28978	37868

This analysis reveals that aside from the rigid body mode, the lowest frequency of the flexible modes is around 400 [Hz], which is much above the frequencies that are usually dealt with in any estimator and controller design. As such, we will only consider the rigid body mode for the gapping mode (i.e., assume all other frequencies to be much higher). Therefore, the kinematic relationships Eq. (12)-(14) and the dynamic equation (22) for the rigid PGT still remain valid. Furthermore, the rigid contact assumption between the brake caliper and the brake disk rotor indicates that $z_b = \dot{z}_b = \ddot{z}_b = 0$, and the rigid nut-screw transmission leads to

$$z_s = \left(\frac{p}{2\pi}\right)\left(\frac{r_s}{2r_n}\right)\theta_s \tag{23}$$

As the inertia effect and viscous damping force of the spindle are negligible, from Eq. (9), $F_{ns} \approx F_{sp1} = 0$, which leads to the following gapping mode model from Eq. (22):

$$J_{geq}\ddot{\theta}_s = T_m - C_{geq}\dot{\theta}_s - \mathrm{sgn}(\dot{\theta}_s)\bullet M_{geq0} \tag{24}$$

Neglecting the gear friction losses, the corresponding values for each of the terms in Eq. (24) for the nominal parameter values can be obtained by using the expression in Eq. (18). As with the results in Table 2, the inertia of sun gear J_s is the most dominant due to the square of gear ratio and pitch ratio. Thus we have the assumption:

$$J_{geq} \cong J_{ceq} \tag{25}$$

A similar relationship for friction losses are obtained by

$$C_{geq} \cong C_{ceq} \quad \text{and} \quad M_{geq0} \cong M_{ceq0} \tag{26}$$

Therefore, the simplified gapping model of Eq. (24) can be seen to be identical to the simplified clamping model of Eq. (22) except for the translational massless brake movement which generates clamping force. Note that Eq. (26) is only valid when the load dependent friction losses are ignored.

5. SIMULATION for MODEL VALIATION

In this section, simulation results for nonlinear and linear models are presented. The nonlinear simulation results show that the model is able to reproduce various nonlinear characteristics such as gap clearance, Coulomb friction, and hysteresis curve. Then, the clamping force and the spindle position are estimated based on the linearized models assuming that the gap clearance and total stiffness are known.

5.1 Nonlinear Simulation for Full Model

For the nonlinear simulation, a step type of open loop motor voltage input is given as 20 [V] to generate and release a typical clamping force, as shown in Fig. 7. Corresponding to a positive voltage input, the spindle position is increased until it contacts the rotor disk. Then, the clamping force also increases following an initial delay to overcome 0.5 [mm] clearance gap between pad and disk rotor. Note that the rate of change in spindle position is decreased due to the clamping load. Corresponding to the subsequent negative voltage input, the spindle position and clamping forces are released. However, the spindle position does not return to its original position due to the retracting force and various nonlinear characteristics of brake assembly. This is one of reasons why the clearance gap management is required with the clamping force feedback control in the future.

Fig. 8 shows a hysteresis curve existing between motor angular position and clamping force which is common in brake assembly due to the Coulomb friction losses. This hysteresis is generated after overcoming the clearance gap. An additional hysteresis curve (dotted line) is presented assuming that the brake pad is exposed to the 200% pad stiffness variation through pad wear and thermal exchange [1].

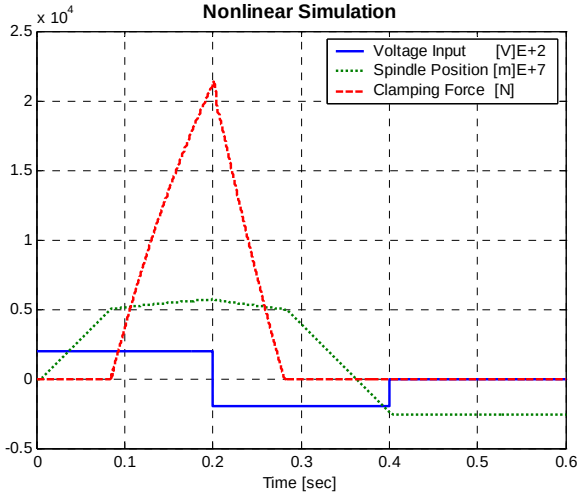

Figure 7. Simulation Results for Nonlinear Full Model

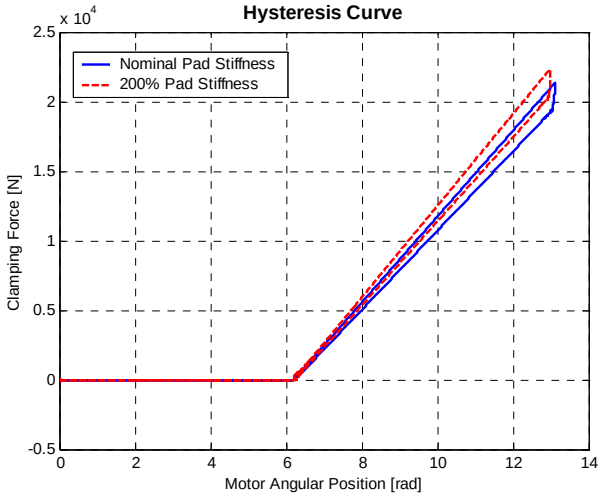

Figure 8. Hysteresis Curve between Motor Angular Position and Clamping Force.

5.2 Linear Simulation for Simplified Models

Based on the simplified models derived in section 4, the clamping force and spindle position can be estimated assuming that the gap clearance and total stiffness are known. To verify the accuracy of Eq. (20) for clamping force estimation, square wave type of open loop motor voltage inputs with 1 [Hz], 5 [Hz], and 10 [Hz] are given to the actuator. Fig. 9 shows that all estimated clamping forces follow the measured clamping forces with small absolute error. Here, by "measured" we mean the results of simulations from the complete (8 DOF) model for system. This means that the assumption of a series connected brake spring and rigid PGT is reasonable for the estimation of the clamping force. However, the relative error is increased on small clamping force actuation due to the ignored stiffness and dynamics. Note also that the clamping force is estimated here without gap clearance (BG=0) between the actuator side pad and the rotor disk.

By Eq. (23), the spindle position can be obtained from the motor position. However, this relationship is only valid while the spindle makes no contact with the disk rotor. Open loop motor voltage inputs for several frequencies (square types in 1 [Hz], 5 [Hz], and 10 [Hz]) are given to generate spindle position without contacting. As shown in Fig. 10, all cases have similar absolute estimation errors. The estimation errors are mainly caused by the neglected backlash of the gear and nut-screw transmissions. Because of this, the estimation error does not decrease when the command spindle position becomes smaller. Overall, the estimation errors for all test cases are within the same level of tolerance as the assumed backlashes, indicating the practical possibility of estimating the spindle position based on the motor angle measurement.

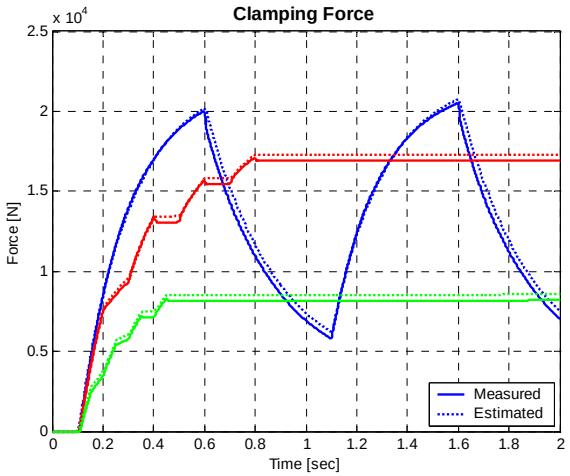

Figure 9. Clamping Force Estimation for Open Loop Input

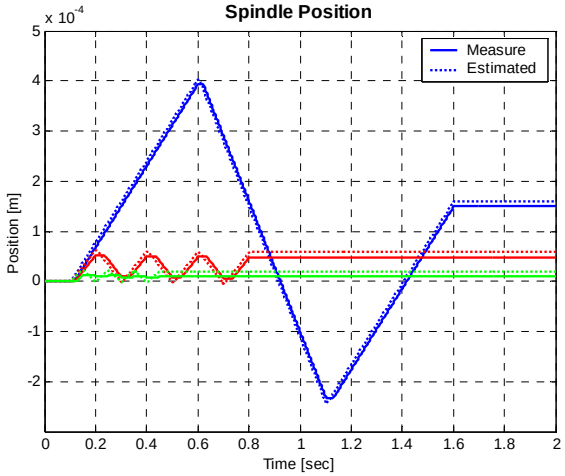

Figure 10. Spindle Position Estimation for Open Loop Input

6. CONCLUSION

A detailed analytical model for electromechnical brake is developed in early design stage, including essential nonlinear characteristics such as backlash, Coulomb friction and gap clearance. The linearized version of the full nonlinear model is then obtained for its modal properties to understand the modes that are critical to the low frequency dynamics of the overall system. The results of the modal analyses are subsequently utilized to reduce the order of PGT model for dynamic simulations and to obtain two simplified models, one for non-contact mode and the other for the contact mode of the

operation. The main difference between the two models is characterized by clamping force load. The derived two simplified models well capture the spindle position and clamping force of the system over the frequency range of interest. These model are now being used in the controller (e.g., clamping force control) and estimator (e.g., gap clearance estimation) designs that are under investigation.

ACKNOWLEDGEMENT

The authors gratefully acknowledge Christopher S. Keeney, Senior Principal Engineer; Dennis A. Kramer, Senior Program Manager; and John Grace, Vice President of Light Vehicle System with ArvinMeritor in Troy, MI for their financial and technical support of this research.

REFERENCE

[1] R. Schwarz, "Reconstruction of the Braking Force in Vehicles with Electromechanically Operated Brakes," Technical Report VDI, No. 393, Technical University of Darmstadt, Germany, 1999 (German).

[2] R. Schwarz, R. Iserman, J. Bohm, J. Nell, and P. Rieth, "Modeling and Control of an Electromechanical Disk Brake," SAE 980600, Detroit, 1998.

[3] C. Maron, T. Dieckmann, S. Hauck, and H. Prinzler, "Electromechnical Brake System: Actuator Control Development System," SAE 970814, Detroit, 1997.

[4] E.G.M.Holweg, R.L.Klomp, J.B.Klaassens, and E.A.Lomonova, "Modeling and Inverse Model-Based Control of an Electro-Mechanical Brake Actuator," 1st IFAC Conference on Mechatronic Systems, Darmstadt, Germany, September 18-20, Volume I, pp39-44, 2000.

[5] W. D. Jonner, H. Winner, L. Dreilich, and E. Schunck, "Electrohydraulic Brake System-The Approach to Brake-by-Wire Technology," SAE960991, Detroit, 1996.

[6] D. E. Schenk, R. L. Wells, and J. E. Miller,"Intelligent Braking for Current and Future Vehicles," SAE950762.

[7] B. Breuer, M. Barz, K. Bill, S. Gruber, M. Semsch, T. Strothjohann, and C. Xie, "The Mechanical Vehicle Corner of Darmstadt University of Technology-Interaction and Cooperation of Sensor Tire, New Low-Energy Disk Brake and Smart Wheel Suspension," International Journal of Automotive Technology, Vol. 3, No. 2, pp63-70, 2002.

[8] R. Kasuba and R. August, "Gear Mesh Stiffness and Load Sharing in Planetary Gearing," ASME, 84DET229, pp348-353.

[9] R. August, R. Kasuba, J. L. Frater, and A. Pintz, "Dynamics of Planetary Gear Train," NASA CR 3793, June 1984.

[10] A. Kahraman, "Planetary Gear Train Dynamics," ASME Journal of Mechanical Design, Vol. 116, pp713-720, Sep. 1994.

[11] Kahraman, "Natural Modes of Planetary Gear Trains," Journal of Sound and Vibration, Vol. 173, pp125-130, 1994.

[12] A. Kahraman, "Free Torsional Vibration Characteristics of Compound Planetary Gear Sets," Mechanism and Machine Theory, Volume 36, Issue 8, pp953-971, August 2001.

[13] J. Lin and R. G. Parker, "Analytical Characterization of the Unique Properties of Planetary Gear Free Vibration," ASME Journal of Mechanical Design, Vol. 121, pp316-321, July 1999.

APPENDIX [A] Complete BBW Model

Sun Gear (Motor Rotor)

$$J_s\ddot{\theta}_s + C_s\dot{\theta}_s + C_{sn}\left(\dot{\theta}_s - \dot{\theta}_n\right) + sgn(\dot{\theta}_s)\left[M_{s0} + M_{sg1}\left(r_s k_{sp}\left|f_{sp1}\right| + r_s c_{sp}\left|f_{sp2}\right|\right)\right] + r_s k_{sp} f_{sp1} + r_s c_{sp} f_{sp2} = T_m$$

$$f_{sp1} = \begin{cases} 0 & for\ \ (r_s\theta_s - r_s\theta_c - r_p\theta_p) < \left|B_{sp}\right| \\ (r_s\theta_s - r_s\theta_c - r_p\theta_p - B_{sp}) & for\ \ (r_s\theta_s - r_s\theta_c - r_p\theta_p) \geq B_{sp} \\ (r_s\theta_s - r_s\theta_c - r_p\theta_p + B_{sp}) & for\ \ (r_s\theta_s - r_s\theta_c - r_p\theta_p) \leq -B_{sp} \end{cases}$$

$$f_{sp2} = \begin{cases} 0 & for\ \ (r_s\theta_s - r_s\theta_c - r_p\theta_p) < \left|B_{sp}\right| \\ (r_s\dot{\theta}_s - r_s\dot{\theta}_c - r_p\dot{\theta}_p) & for\ \ (r_s\theta_s - r_s\theta_c - r_p\theta_p) \geq \left|B_{sp}\right| \end{cases}$$

Planetary Gear (Rotation)

$$J_p(\ddot{\theta}_p - \ddot{\theta}_c) + C_p\dot{\theta}_p + sgn(\dot{\theta}_p)\left[M_{p0} + M_{pg1}\left(r_p k_{pr}\left|f_{pr1}\right| + r_p c_{pr}\left|f_{pr2}\right|\right)\right] + r_p k_{pr} f_{pr1} + r_p c_{pr} f_{pr2} - r_p k_{sp} f_{sp1} - r_p c_{sp} f_{sp2} = 0$$

$$f_{pr1} = \begin{cases} 0 & for\ \ \left|(r_p\theta_p - (r_n + r_p)\theta_c\right| < B_{pr} \\ (r_p\theta_p - (r_n + r_p)\theta_c - B_{pr}) & for\ \ (r_p\theta_p - (r_n + r_p)\theta_c) \geq B_{pr} \\ (r_p\theta_p - (r_n + r_p)\theta_c + B_{pr}) & for\ \ (r_p\theta_p - (r_n + r_p)\theta_c) \leq -B_{pr} \end{cases}$$

$$f_{pr2} = \begin{cases} 0 & for\ \ \left|(r_p\theta_p - (r_n + r_p)\theta_c\right| < B_{pr} \\ (r_p\dot{\theta}_p - (r_n + r_p)\dot{\theta}_c) & for\ \ \left|(r_p\theta_p - (r_n + r_p)\theta_c\right| \geq B_{pr} \end{cases}$$

Planetary Gear (Revolution)

$$(J_p + m_p r_n^2)\ddot{\theta}_c - J_p\ddot{\theta}_p + r_n k_{pn} f_{pn1} + r_n c_{pn} f_{pn2} - C_p\dot{\theta}_p - sgn(\dot{\theta}_p)[M_{p0} + M_{pg1}\left(r_p k_{pr}\left|f_{pr1}\right| + r_p c_{pr}\left|f_{pr2}\right|\right)] - r_s k_{sp} f_{sp1} - r_s c_{sp} f_{sp2} - (r_n + r_p)k_{pr} f_{pr1} - (r_n + r_p)c_{pr} f_{pr2} = 0$$

$$f_{pn1} = \begin{cases} 0 & for\ \ r_n\left|(\theta_c - \theta_n)\right| < B_{pn} \\ r_n(\theta_c - \theta_n) - B_{pn} & for\ \ r_n(\theta_c - \theta_n) \geq B_{pn} \\ r_n(\theta_c - \theta_n) + B_{pn} & for\ \ r_n(\theta_c - \theta_n) \leq -B_{pn} \end{cases}$$

$$f_{pn2} = \begin{cases} 0 & for\ \ r_n\left|(\theta_c - \theta_n)\right| < B_{pn} \\ r_n(\dot{\theta}_c - \dot{\theta}_n) & for\ \ r_n\left|(\theta_c - \theta_n)\right| \geq B_{pn} \end{cases}$$

Nut Carrier

$$J_n\ddot{\theta}_n + C_n\dot{\theta}_n + C_{sn}(\dot{\theta}_n - \dot{\theta}_s) + sgn(\dot{\theta}_n)\left[M_{n0} + M_{n1}\left(K_{ns}\left|f_{ns1}\right| + C_{ns}\left|f_{ns2}\right|\right)\right] + \left(\frac{p}{2\pi}\right)(K_{ns} f_{ns1} + C_{ns} f_{ns2}) - r_n k_{pn} f_{pn1} - r_n c_{pn} f_{pn2} = 0$$

$$M_{n1} = M_{nb1}\left(r_n\frac{2\pi}{p}\right) + M_{ng1}$$

$$f_{ns1} = \begin{cases} 0 & for\left|(\frac{p}{2\pi}\theta_n + z_b - z_s)\right| < B_{ns} \\ (\frac{p}{2\pi}\theta_n + z_b - z_s - B_{ns}) & for\ \ (\frac{p}{2\pi}\theta_n + z_b - z_s) \geq B_{ns} \\ (\frac{p}{2\pi}\theta_n + z_b - z_s + B_{ns}) & for\ \ (\frac{p}{2\pi}\theta_n + z_b - z_s) \leq -B_{ns} \end{cases}$$

$$f_{ns2} = \begin{cases} 0 & for\left|(\frac{p}{2\pi}\theta_n + z_b - z_s)\right| < B_{ns} \\ (\frac{p}{2\pi}\dot{\theta}_n + \dot{z}_b - \dot{z}_s) & for\left|(\frac{p}{2\pi}\theta_n + z_b - z_s)\right| \geq B_{ns} \end{cases}$$

Spindle

$$m_{sp}\ddot{z}_s + C_{sb}(\dot{z}_s - \dot{z}_b) + K_{sp1} ff_{sp1} + C_{sp1} ff_{sp2} - K_{ns} f_{ns1} - C_{ns} f_{ns2} = 0$$

$$ff_{sp1} = \begin{cases} 0 & for\ \ z_s < BG \\ z_s - BG & for\ \ z_s \geq BG \end{cases}$$

$$ff_{sp2} = \begin{cases} 0 & for\ \ z_s < BG \\ \dot{z}_s & for\ \ z_s \geq BG \end{cases}$$

Brake Caliper

$$m_b\ddot{z}_b + C_{sb}(\dot{z}_b - \dot{z}_s) + K_c z_b + C_c\dot{z}_b + \mathrm{sgn}(\dot{z}_b)\left(F_{bt0} + \mu_b\mu_c\left|F_{sp1}\right|\right) + F_{ns} = 0$$

APPENDIX [B] Nomenclature and Parameters

Inertia and Mass (i=1~3)		**Value**
Rotor Inertia (Sun Gear)	J_s [kgm^2]	2.112E-4
Planetary Gear Inertia ($J_{pi} = J_p/3$)	J_p [kgm^2]	1.410E-6
Planetary Gear Mass ($m_{pi} = m_p/3$)	m_p [kg]	2.340E-2
Nut Inertia	J_n [kgm^2]	3.199E-4
Spindle Mass with Pad	m_{sp} [kg]	5.380E-1
Brake Caliper Mass	m_b [kg]	6.410

Contact & Structural Stiffness (i=1~3)		**Value**
Sun-Planetary Gear ($k_{spi} = k_{sp}/3$)	k_{sp} [N/m]	3.000E+8
Planetary-Ring Gear ($k_{pri} = k_{pr}/3$)	k_{pr} [N/m]	4.500E+8
Planetary Gear-Nut ($k_{pni} = k_{pn}/3$)	k_{pn} [N/m]	9.000E+7
Roller Screw Stiffness	K_{ns} [N/m]	3.000E+9
Pad Stiffness (per piece)	K_p [N/m]	3.000E+8
Caliper Stiffness	K_c [N/m]	4.286E+7

Backlash and Gap		**Value**
Sun-Planetary	B_{sp} [m]	0.0001
Planetary-Ring	B_{pr} [m]	0.0001
Planetary-Nut	B_{pn} [m]	0.0001
Nut-Screw	B_{ns} [m]	0.0001
Disk Gap	BG [m]	0.0005

Radius (i=1~3)		**Value**
Sun Gear	r_s [m]	0.022
Planetary Gear	r_{pi} [m]	0.010
Nut Carrier	r_n [m]	0.032

Sun	Bearing friction	C_s [Nms/rad]	0.001
	Bearing friction between sun gear and nut	C_{sn} [Nms/rad]	0.001
	Static friction	M_{s0} [Nm]	0.100
	Load friction	M_{s1} [-]	0.010
Planetary	Bearing friction	C_p [Nms/rad]	0.001
	Static friction	M_{p0} [Nm]	0.100
	Load friction	M_{p1} [-]	0.010
Nut	Bearing friction	C_n [Nms/rad]	0.002
	Static friction	M_{n0} [Nm]	0.200
	Load friction	M_{n1} [-]	0.020

Contact & Structural Damping (i=1~3)		**Value**
Sun-Planetary Gear($c_{spi} = c_{sp}/3$)	c_{sp} [Ns/m]	204.57
Planetary-Ring Gear ($c_{pri} = c_{pr}/3$)	c_{pri} [Ns/m]	204.57
Planetary Gear-Nut($c_{pni} = c_{pn}/3$)	c_{pn} [Ns/m]	111.84
Nut-Roller Screw	C_{ns} [Ns/m]	1270
Pad (per piece)	C_{sp} [Ns/m]	3000
Spindle and Caliper	C_{sb} [Ns/m]	7000
Brake Caliper Damping	C_c [Ns/m]	3500

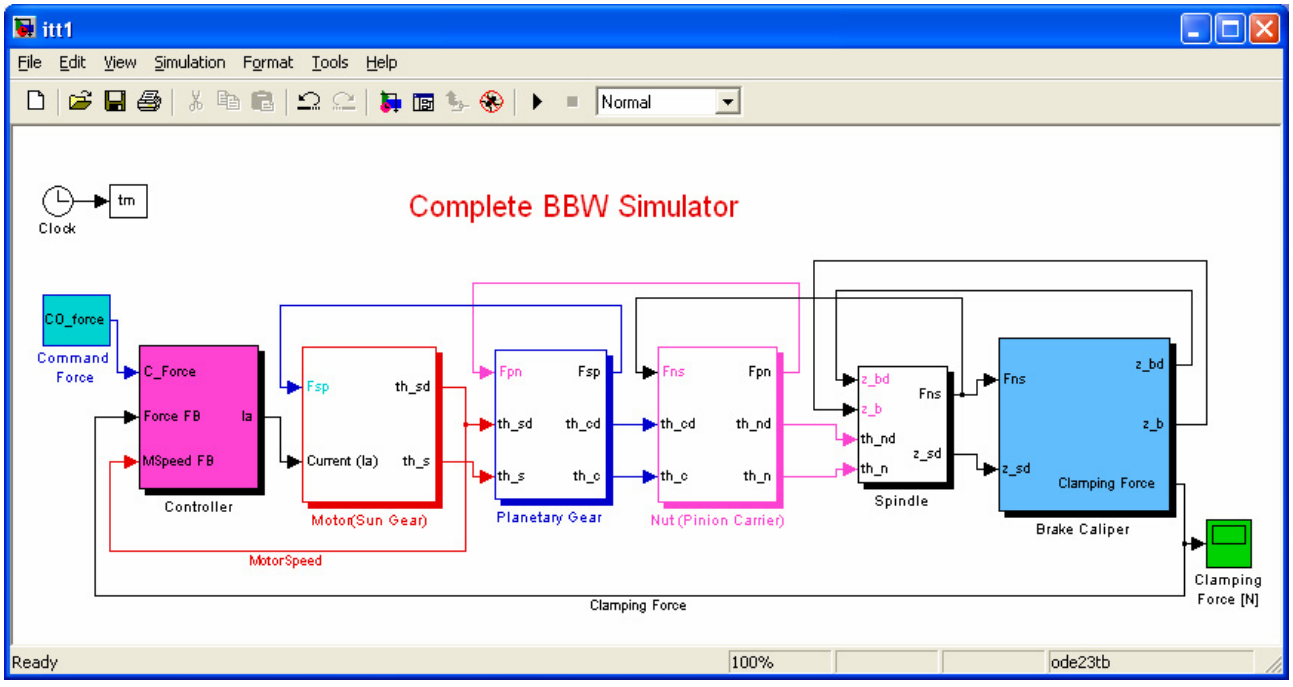

Figure 11. SIMULINK Block for Complete Electromechanical Brake System